Science Advances

AAAS

advances.sciencemag.org/cgi/content/full/2/12/e1601742/DC1

Supplementary Materials for

Butterfly magnetoresistance, quasi-2D Dirac Fermi surface and topological phase transition in ZrSiS

Mazhar N. Ali, Leslie M. Schoop, Chirag Garg, Judith M. Lippmann, Erik Lara, Bettina Lotsch, Stuart S. P. Parkin

Published 16 December 2016, *Sci. Adv.* **2**, e1601742 (2016)
DOI: 10.1126/sciadv.1601742

This PDF file includes:

SUPPLEMENTARY INFORMATION FOR: BUTTERFLY MAGNETORESISTANCE, QUASI-2D DIRAC FERMI SURFACE AND A TOPOLOGICAL PHASE TRANSITION IN ZRSIS

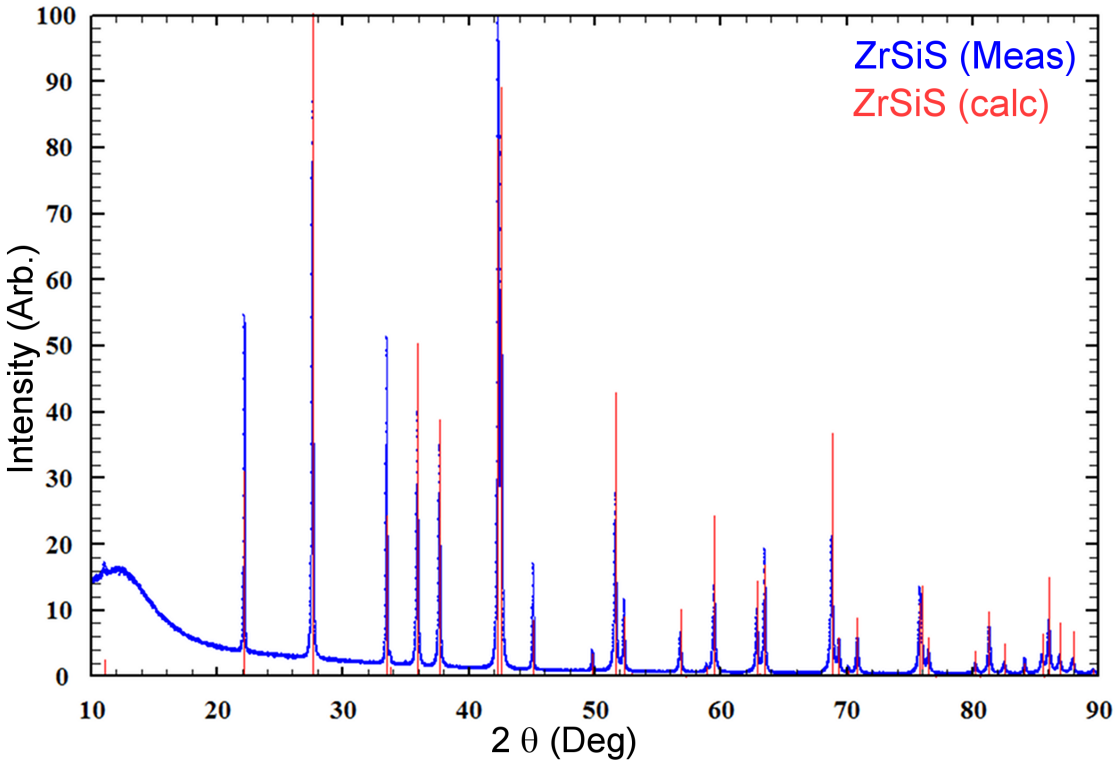

fig. S1. **Powder x-ray diffraction pattern for ground single crystals of ZrSiS (color online):** The blue pattern shows the measured data at room temperature using Cu-Kα radiation while the red bars show the calculated pattern. The differences in intensities are expected due to preferred orientation effects of the plate-like crystals. Single crystal XRD has been done on crystals from the same batch and published elsewhere [12].

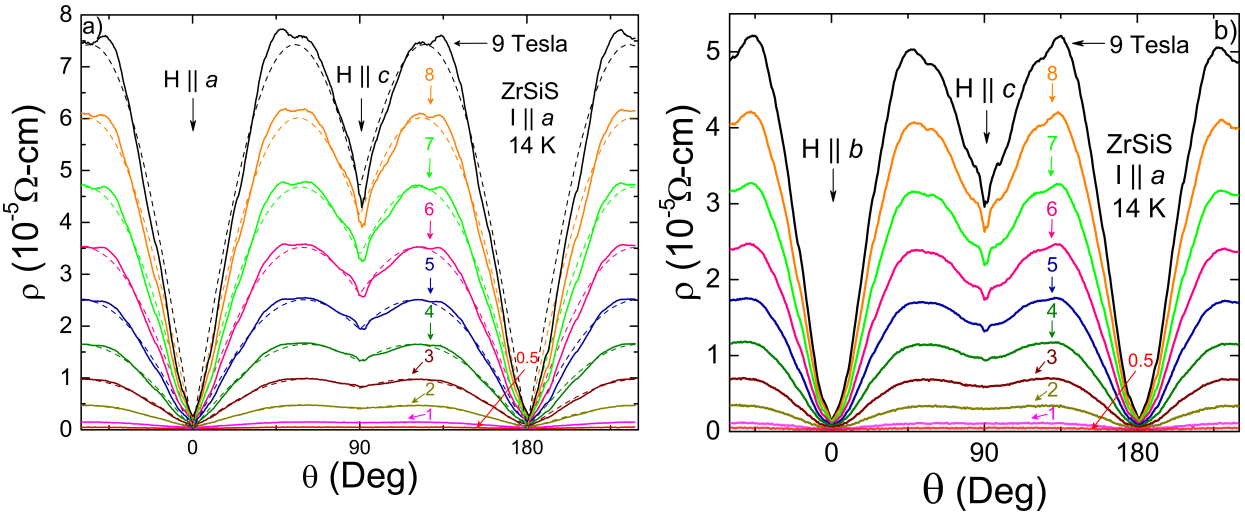

fig. S2. **AMR measured in other principal directions along with symmetry fitting. (color online):** Panel (**A**) shows the AMR when I is || a and H is swept from H || c to a. The solid lines are the data while dashed lines represent the fit to $\rho_\theta = p_1 * sin(\theta)^2 + p_2 * sin(2\theta)^2 + 1$. The absolute quantitative agreement of the fit is low due to the the peak splitting present around 45°, the dip around 90° and other oscillatory components. The fit extracts only the weight of the 2−fold and 4−fold components and ignores the other components. This analysis was carried out on data sets taken at 14 K, 20 K, 25 K, 30 K, 50 K, and 70 K. Panel (**B**) shows the AMR when I is || a and H is swept from H || c to b instead of a. This shows that the effect is symmetric with the ab plane. The MR is lower as the crystal was damaged by dismounting, re-contacting, and then remounting the crystal after rotating 90°.

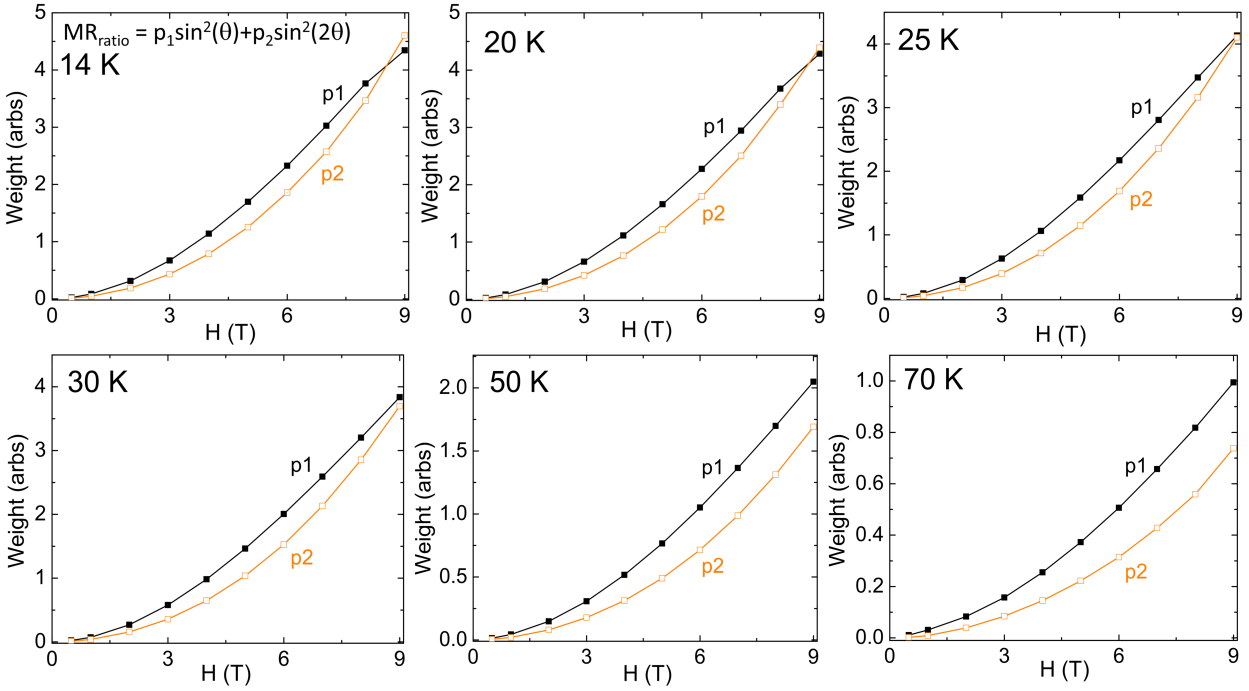

fig. S3. **Extracted weights from AMR fitting (color online):**
The panel shows the extracted weights of the 2-fold and 4-fold symmetry components of each AMR loop between 0.5 and 9 T, at various temperatures obtained by fitting the data to a simple trigonometric equation. The θ and 2θ components show significantly different temperature dependencies.

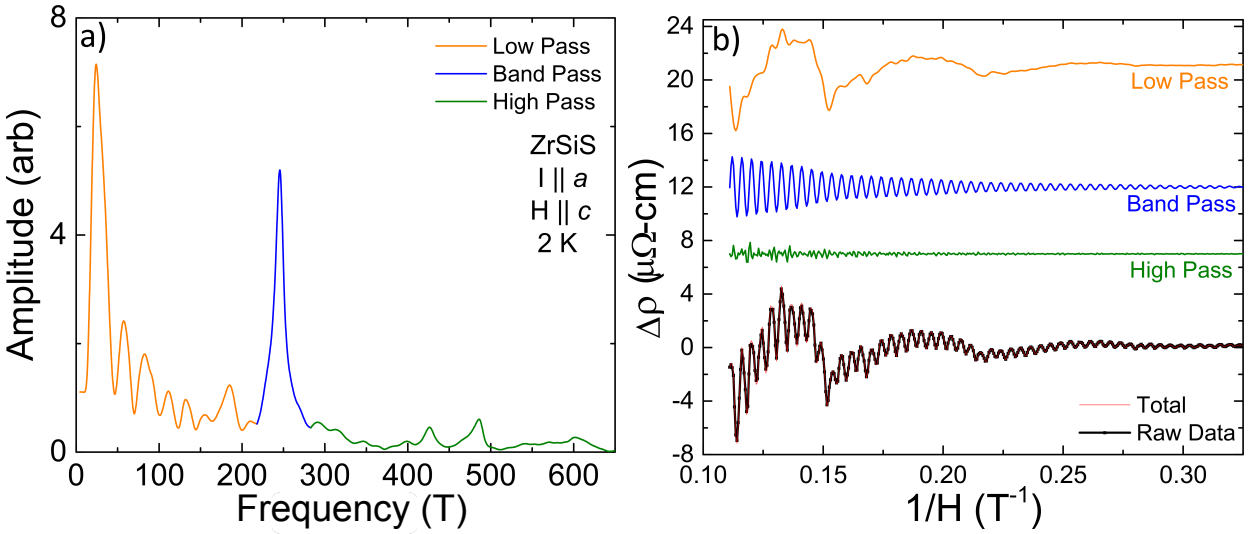

fig.S4. Quantitative quantum oscillation analysis using band pass filtration. (color online): Panel **(A)** To resolve and analyze the multiple SdH oscillations in our MR data, we have taken a fast Fourier transform (FFT) which yields information identifying frequencies of the multiple Fermi pockets. Panel **(A)** shows a representative FFT of the SdH oscillations taken at H || *c*. A forward-backward band-pass Butterworth filter was then applied between the cutoff frequencies 218.09T and 283.06T (the bandwidth of the band pass filter is indicated in blue) to extract the oscillations of the 243T peak. The filtering was done using MATLABs filtfilt routine which does filtering in both forward and backward directions to achieve zero phase shift. Four steps (filter, reverse, filter, reverse) are used. To understand this, if we consider that x(n) is the input signal and g(n) is the filters impulse response at sample "n", then the application of the filter will result in X($e^{i\theta}$)*G($e^{i\theta}$) in the frequency domain. Here, X($e^{i\theta}$) is the Fourier transform of x(n) and G($e^{i\theta}$) is the Fourier transform of g(n). To do the backwards filtering, we first do a time reversal operation to get X($e^{-i\theta}$)*G($e^{-i\theta}$) and subsequently reapply the filter to yield this term: X($e^{-i\theta}$)G($e^{i\theta}$)G($e^{-i\theta}$), which is equivalent to X($e^{i\theta}$)*$|G(e^{i\theta})|^2$. (For real-valued time functions, the Fourier transform is conjugate symmetric, hence, G($e^{-i\theta}$) = G*(complexconjugate)($e^{-i\theta}$) and G($e^{i\theta}$)G($e^{-i\theta}$) = $|G(e^{i\theta})|^2$. Thus, forward-backward filtering squares the filters amplitude response and zeroes the phase shift [42–44]. A higher order Butterworth filter was used in this instance. The order of the filter is determined based on the presence of any peaks in the vicinity. A higher order filter gives a sharper transition around the cutoff frequency but can also introduce ringing or unintended distortion in the reciprocal field domain so a compromise is often necessary. Similarly, oscillations in other ranges of frequencies were extracted using low-pass and high-pass filters and their bandwidth is indicated by the color coding in the figure S4a. After the forward-backward filtering, the signal was re-transformed back into the reciprocal field domain, as shown in panel b). All the filtered components are added together (in red) and overlayed with the raw signal (in black) to confirm that no phase shifts or signal distortions were introduced during the filtering process.

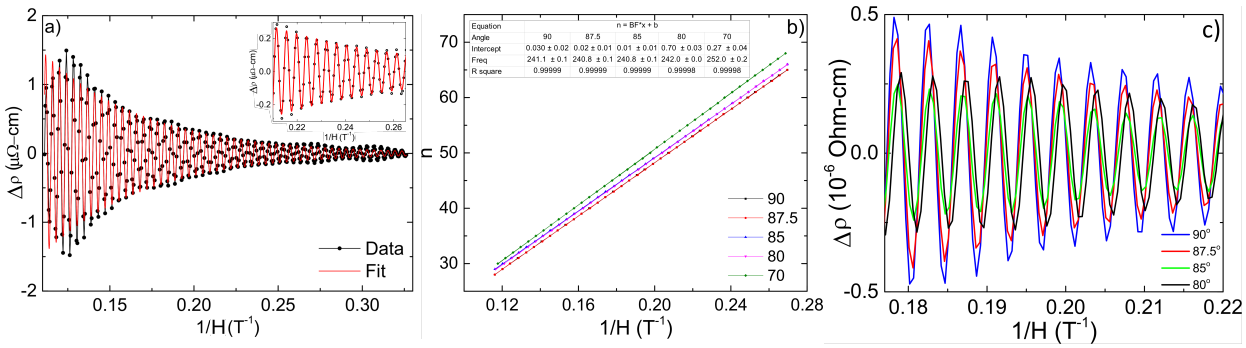

fig. S5. Direct Lifshitz-Kosevich fitting compared with Landau Level fan diagram

Panel **(A)** shows the extracted oscillations (black circles) for F_β at 90° and 2K. We fit it to the Lifshitz-Kosevich formula: $\frac{\Delta\rho}{\rho} \approx e^{-\lambda_D}\frac{\lambda}{\sinh(\lambda)}\cos(2\pi(\frac{B_F}{B}+p)$, where $\lambda_D = \frac{2\pi^2 m_c k_b T_D}{heB}$. The thermal damping factor, $\lambda = \frac{2\pi^2 m_c k_b T}{heB}$, m_c is the cyclotron mass of the electron, T_D is the Dingle temperature, B_F is the magnetic frequency, and p is the total phase, equal to $\gamma - \delta$. T_D, B_F, and p are the refined parameters. We find a good fit (red line) to the data (with an R^2 value of 0.98) as is better seen in the inset. Panel **(B)** shows the Landau Level index fan diagram, constructed using the oscillation maximas for F_β for the angles 90, 87.5, 85, 80 and 70°. The phase obtained from the LL index fit has a very close agreement with the aforementioned LK fit. Panel **C**) overlays the extracted oscillations for F_β at various angles and illustrates the sudden change in phase which occurs by 80°.